STRUCTURAL CHEMISTRY

ISSN 2053-2296

Received 7 July 2026
Accepted 17 August 2026

Edited by M. Rosales-Hoz, Cinvestav, Mexico

This article is part of the collection *Early Career Scientists in Structural Science*.

**Keywords:** crystal structure; thallium(I) salts; weakly coordinating anion; supramolecular interactions; anisotropic thermal expansion.

**CCDC reference:** 2581457

**Supporting information:** this article has supporting information at journals.iucr.org/c

# Solvent-free thallium(I) tetrakis[3,5-bis(trifluoromethyl)phenyl]borate: crystal structure, supramolecular interactions and anisotropic thermal expansion

**Johannes Stephan,[a,b]* Lena Schröck,[a,b] E. Eja Petersen,[b] Romy L. Ettlinger[b] and Alexander Pöthig[a]**

[a]Catalysis Research Center, Technical University of Munich, Ernst-Otto-Fischer-Straße 1, Garching, 85748, Germany, and [b]Chair of Inorganic and Metal-Organic Chemistry, TUM School of Natural Sciences, Technical University of Munich, Lichtenbergstraße 4, Garching, 85748, Germany. *Correspondence e-mail: johannes.stephan@tum.de

Thallium salts of weakly coordinating anions are common reagents in organometallic chemistry for generating reactive cationic species *via* salt metathesis. Despite their frequent use, their composition is often ambiguous due to cocrystallized solvents, rendering well-characterized solvent-free structures rare. Herein, we report the synthesis, crystal structure and thermal properties of truly solvent-free thallium(I) tetrakis[3,5-bis(trifluoromethyl)phenyl]borate, $Tl[BC_{32}H_{12}F_{24}]$, as determined by single-crystal X-ray diffraction (SC-XRD), powder X-ray diffraction (PXRD) and thermogravimetric analysis (TGA). The structure features short Tl···F contacts and a complex supramolecular architecture that is closely related to disorder and tilting of the anion arene rings, which generate distinct intermolecular interaction motifs. Key features include a herringbone arrangement of nonclassical C—H···F hydrogen bonds and a 'fluorous' interlayer defined by F···F and C—F···$\pi$ contacts. This leads to hinge-like networks in the structure, depending on the tilt of the arene rings. These features are associated with anisotropic thermal expansion, with significantly greater expansion along the crystallographic *a* and *b* axes, as inferred from PXRD measurements. In agreement with the solvent-free structure determined by SC-XRD, TGA confirms that the bulk material is solvent-free.

## 1. Introduction

Owing to their high chemical stability and their low nucleophilicity, weakly coordinating anions (WCAs) have significantly influenced coordination chemistry over the last three decades (Krossing & Raabe, 2004; Riddlestone *et al.*, 2018). In particular, their ability to generate reactive cationic species without masking the cation's reactivity through undesirable coordination has made them valuable building blocks for, *e.g.* catalysis, bond-activation reactions and electrochemistry. Prime examples of reactive cationic compounds, stabilized by WCAs, include the silylium ion (Kim *et al.*, 2002), the nonclassical 2-norbornyl carbocation (Scholz *et al.*, 2013), as well as metals in uncommon environments or oxidation states, such as metal–alkane complexes (Evans *et al.*, 1997; Pike *et al.*, 2012) or an $Au^{II}$ centre with unusual ligands (Seidel & Seppelt, 2000). Among the numerous WCAs reported to date (Reed, 1998; Krossing, 2001; Kelling *et al.*, 2024; He *et al.*, 2025), the tetraarylborate anions tetrakis[3,5-bis(trifluoromethyl)phenyl]borate ($BAr^F$) (Nishida *et al.*, 1984) and tetrakis(pentafluorophenyl)borate, $[B(C_6F_5)_4]^-$ (Massey & Park, 1964; Lambert & Zhang, 1993), represent some of the most frequently employed representatives, owing to their

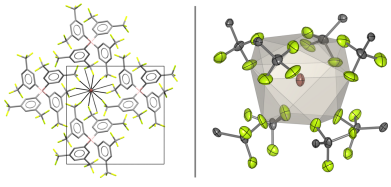

excellent weakly coordinating properties and straightforward preparation.

WCAs are typically introduced *via* salt metathesis or halide abstraction reactions, for which application silver and thallium salts have proven particularly useful reagents (Heintz *et al.*, 2002). Their utility arises from the favourable combination of their high solubility in organic solvents and their propensity to form poorly soluble halide salts. Although thallium salts are substantially more toxic than their silver counterparts, they are generally less oxidizing and therefore more redox-innocent reagents. Consequently, thallium WCA salts may provide access to low-valent metal complexes that are difficult to obtain using silver salts, which may otherwise induce undesired oxidation processes (Salem *et al.*, 2008).

Despite their widespread use in synthetic inorganic and organometallic chemistry (Heintz *et al.*, 2002; Alberti & Pörschke, 2004), crystal structures of silver and thallium WCA salts remain comparatively scarce, particularly in the absence of cocrystallized solvent molecules. The weak interactions between the cation and the anion often permit additional stabilization through weak solvent coordination, making solvate formation a common feature of these compounds (McSkimming, 2025; Carreras *et al.*, 2017). As a result, structures of genuinely solvent-free WCA salts are relatively rare, which hampers insight into the intrinsic cation–anion interactions that govern their solid-state structures. Concerning in particular thallium tetraarylborate salts, a solvent-free modification has so far been reported only for $Tl[B(C_6F_5)_4]$ (Parvez *et al.*, 2005). '$Tl(BAr^F)$', in contrast, has previously been described exclusively as a dichloromethane solvate containing 0.33 molecules of dichloromethane per formula unit of $Tl(BAr^F)$ (Hughes *et al.*, 1997).

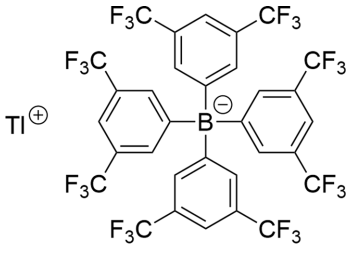


$Tl(BAr^F)$

Scheme 1

In this article, we report the crystal structure and bulk properties of truly solvent-free thallium(I) tetrakis[3,5-bis(trifluoromethyl)phenyl]borate [$Tl(BAr^F)$]. Single-crystal X-ray diffraction (SC-XRD) reveals the solid-state structure of the unsolvated salt and allows a detailed assessment of the weak Tl···F interactions that dominate its crystal packing, amongst weak F···F and C—H···F interactions. Phase purity and bulk crystallinity were confirmed by powder X-ray diffraction (PXRD), while thermogravimetric analysis (TGA) was used to confirm the solvent-free nature of the bulk material and elucidate its thermal stability.

## 2. Experimental

### 2.1. Synthesis and crystallization

Thallium tetrakis[3,5-bis(trifluoromethyl)phenyl]borate was synthesized based on established procedures (Hughes *et al.*, 1997; Alberti & Pörschke, 2004; Stephan *et al.*, 2025). This involves protolysis of thallium(I) ethoxide with $H(Et_2O)(BAr^F)$ (Brookhart's acid). Following the most recent protocol (Stephan *et al.*, 2025), thallium(I) ethoxide (0.2604 g, 1.04 mmol, 1.06 equiv.) was added to a solution of an equimolar amount of Brookhart's acid (1.0032 g, 0.98 mmol, 1.00 equiv.) in dry diethyl ether (5 ml) in a Schlenk tube under an argon atmosphere. After stirring for 10 min at room temperature, all volatiles were removed *in vacuo* to yield a beige powder. Immediately after adding thallium ethoxide, the solution may turn cloudy, presumably because thallium chloride may form from traces of sodium chloride (<1%) in $H(Et_2O)(BAr^F)$. The TlCl precipitate can be easily removed by filtration using a syringe filter inside a glovebox. Redissolving the crude $Tl(BAr^F)$ in dry fluorobenzene (4 ml) and layering the solution with dry *n*-hexane (10 ml) reproducibly yields colourless crystals several millimetre in size at room temperature after 2 to 3 d, with a total yield of 75–85%. Alternatively, smaller-sized crystals can easily be obtained by cooling a $Tl(BAr^F)$ solution in a 1:1 mixture (8 ml) of fluorobenzene and *n*-hexane to −32 °C overnight with identical yield and properties.

For SC-XRD analysis, $Tl(BAr^F)$ single crystals were selected in an argon-filled glovebox with appropriate dust filters (to prevent atmospheric contamination with thallium) and covered in perfluorinated ether on a microscope slide inside the glovebox. A suitable single crystal was then mounted on a MicroMount Kapton microsampler, transferred to the diffractometer and frozen under a stream of cold nitrogen (100 K).

### 2.2. Refinement

Crystal data, data collection and structure refinement details are summarized in Table 1. Anharmonic motion of the Tl atom (Tl1) was refined using a fourth-order Gram–Charlier expansion as implemented in *olex2.refine* (Bourhis *et al.*, 2015) within *OLEX2* (Dolomanov *et al.*, 2009). H atoms were located in difference Fourier maps, but were calculated in ideal positions using a riding model, with C—H = 0.99 Å and $U_{iso}(H) = 1.2U_{eq}(C)$. The disorder of the arene rings of the $BAr^F$ anions over three positions, tilted by 5.49 and 6.15°, was modelled using a split-layer refinement, and the geometry of the second and third component with minor occupancy were restrained to be the same as in PART 1. To ensure convergence, restraints were used within reasonable limits. Additionally, the C—F bond lengths for the $CF_3$ groups of the parts with minor occupancy were restrained to 1.34 (2) Å. The carbon frameworks of the two parts with minor occupancies, except for the F atoms, were modelled as rigid bodies. Thermal displacement parameters for certain F atoms were constrained to be equal to their counterparts in PART 1, as well as the

boron-bound C atoms, which were constrained to be equal to C1 (PART 1).

### 2.3. Powder X-ray diffraction

Powder X-ray diffraction data were acquired using sealed borosilicate glass capillaries with a diameter of 0.5 mm, filled under an argon atmosphere in a glovebox with appropriate dust filters. Intensities were collected at room temperature on a STOE Stadi P two-circle powder X-ray diffractometer with Debye–Scherrer geometry. The diffractometer was equipped with a sealed-tube X-ray source emitting Mo $K\alpha$ radiation, a curved Ge monochromator and a Dectris Mythen2 DCS4 detector. Cell indexing and refinement were performed using *WinXPOW* (Version 3.05; STOE & Cie GmbH, Darmstadt, Germany).

### 2.4. Thermogravimetric analysis

Thermogravimetric analysis (TGA) was performed on a Mettler Toledo TGA/DSC3+ under a constant flow of argon (25 ml min$^{-1}$). A sample of Tl(BAr$^{F}$) was ground in an agate mortar in an argon-filled glovebox and approximately 2 mg were weighed into a calcined alumina crucible, which was placed into the TGA device. Heating was applied in a range between 30 and 1000 °C, with a heating rate of 2 °C min$^{-1}$.

## 3. Results and discussion

Solvent-free Tl(BAr$^{F}$) crystallizes in a primitive tetragonal space group, as derived from SC-XRD. Due to the weakly coordinating nature of the fluorobenzene solvent that was used for crystallization, a structure containing no solvent molecules was obtained. This is supported by PXRD (see Fig. S8 in the supporting information), which shows the same solvent-free unit cell for the bulk material, elemental analysis (see Table S1) and $^{1}$H NMR spectrum in $d_3$-acetonitrile solution (see Fig. S1). The $^{1}$H NMR spectrum shows only two closely adjacent peaks at 7.70 and 7.67 ppm, which can be attributed to the protons of the BAr$^{F}$ anion.

The solvent-free crystal structure of Tl(BAr$^{F}$), as determined by SC-XRD, was modelled in the centrosymmetric tetragonal space group $P4/n$ (No. 85, $Z = 2$) with two formula units per unit cell. In fact, the structure appears to exhibit pronounced pseudocentrosymmetry. Initially, space group determination using *XPREP* (Bruker, 2014) suggested the centrosymmetric space groups $P4/n$ and $P4/nmm$, whereas intensity statistics with $|E^2 - 1| = 0.689$ were indicative of a noncentrosymmetric or chiral space group. Structure solution using *SHELXT* (Sheldrick, 2015*a*) was successful only for the centrosymmetric space group $P4/n$ and the Sohncke space group $P4$. We therefore tested refinement for both solutions and the $P4/n$ structure model proved more accurate. Briefly, refinement in $P4$ converged satisfactorily as a two-component inversion twin with a final BASF $\simeq 0.5$, but yielded only slightly lower $R$ values. However, the Flack (1983) parameter was refined to a statistically significant value of 0.50 (3), indicating inversion ambiguity consistent with a centrosymmetric model, and the *PLATON* ADDSYM analysis (Spek, 2020) also recommended the higher-symmetry space group $P4/n$. The structure model in $P4/n$ (instead of $P4$) additionally yielded physically more reasonable atomic displacement parameters, especially for the light elements boron and carbon. Therefore, the centrosymmetric model was adopted as the more accurate description of the structure.

**Table 1**
Experimental details.

| | |
|---|---|
| Crystal data | |
| Chemical formula | $Tl^{+}\cdot C_{32}H_{12}BF_{24}^{-}$ |
| $M_r$ | 1067.63 |
| Crystal system, space group | Tetragonal, $P4/n$ |
| Temperature (K) | 100 |
| $a$, $c$ (Å) | 13.4930 (4), 9.6227 (5) |
| $V$ (Å$^3$) | 1751.92 (12) |
| $Z$ | 2 |
| Radiation type | Mo $K\alpha$ |
| $\mu$ (mm$^{-1}$) | 4.76 |
| Crystal size (mm) | 0.16 × 0.15 × 0.10 |
| | |
| Data collection | |
| Diffractometer | Bruker D8 VENTURE |
| Absorption correction | Multi-scan (*SADABS*; Bruker, 2016) |
| $T_{min}$, $T_{max}$ | 0.633, 0.747 |
| No. of measured, independent and observed [$I \geq 2\sigma(I)$] reflections | 87174, 3197, 2970 |
| $R_{int}$ | 0.055 |
| $(\sin\theta/\lambda)_{max}$ (Å$^{-1}$) | 0.757 |
| | |
| Refinement | |
| $R[F^2 > 2\sigma(F^2)]$, $wR(F^2)$, $S$ | 0.021, 0.053, 1.06 |
| No. of reflections | 3197 |
| No. of parameters | 284 |
| No. of restraints | 697 |
| H-atom treatment | H atoms treated by a mixture of independent and constrained refinement |
| $\Delta\rho_{max}$, $\Delta\rho_{min}$ (e Å$^{-3}$) | 0.59, −0.86 |

Computer programs: *APEX4* (Bruker, 2022), *SAINT* (Bruker, 2019), *SHELXT* (Sheldrick, 2015*a*), *SHELXL* (Sheldrick, 2015*b*), *ShelXle* (Hübschle *et al.*, 2011), *Mercury* (Macrae *et al.*, 2020), *PLATON* (Spek, 2020), *enCIFer* (Allen *et al.*, 2004) and *FinalCIF* (Kratzert, 2026), *OLEX2* (Dolomanov *et al.*, 2009), *olex2.refine* (Bourhis *et al.*, 2015) and *VESTA 3* (Momma & Izumi, 2011).

Concomitantly, anharmonic motion was refined for the Tl atom using *olex2.refine* (Bourhis *et al.*, 2015), as implemented in the *OLEX2* software package (Dolomanov *et al.*, 2009). Fourth-order anharmonic refinement of the Tl atom resulted in a substantially improved description of the structure, as evidenced by the conventional residual indices decreasing from $R1 = 3.45\%$ and $wR2 = 9.08\%$ for the harmonic model to $R1 = 2.06\%$ and $wR2 = 5.26\%$ for the anharmonic model (see Table 1). In addition, high residual electron density of 7.89 e Å$^{-3}$ in the vicinity of the Tl atom (<1 Å) was virtually completely removed to 0.57 e Å$^{-3}$ in the anharmonic model. Although the resolution criterion proposed by Kuhs (1988), which recommends a minimum resolution of 0.58 Å for reliable fourth-order anharmonic refinement, is not fulfilled with 0.66 Å, the anharmonic model appears physically meaningful. The resulting probability density function remained positive throughout the inspected region (see Fig. S7), and only a limited number of Gram–Charlier coefficients were found to be statistically significant. The expansion is dominated by the

**Table 2**
Selected interatomic distances (Å), suggesting a nonclassical C—H···F hydrogen bond, as well as weak F···F and C—F···$\pi$ interactions.

| | | | |
|---|---|---|---|
| H6···F1$^{ii}$ | 2.621 (7) | F5$A$···C5$A^{iii}$ | 3.153 (8) |
| F3$A$···F4$A^{i}$ | 2.90 (3) | F5$B$···C4$B^{iii}$ | 3.195 (12) |
| F5$A$···C4$A^{iii}$ | 3.180 (9) | F5$B$···C5$B^{iii}$ | 3.182 (12) |

Symmetry codes: (i) $-x+1, -y+1, -z+1$; (ii) $-y+\frac{3}{2}, x, z$; (iii) $y+\frac{1}{2}, -x+1, -z+1$.

third-order C333 coefficient [$-4.11\ (8) \times 10^{-6}$; $51.4\sigma$], while for the fourth-order terms, D3333 [$4.20\ (11) \times 10^{-7}$; $38.2\sigma$], represents the dominant contribution. All remaining coefficients are either symmetry-restricted, statistically insignificant or (marginally) significant at the $10\sigma$ level. For this reason, the anharmonic model was adopted as a valid and more realistic representation of Tl atomic motion. More details on refinement and the Gram–Charlier coefficients can be found in the supporting information (see Tables S2 and S3).

The asymmetric unit of Tl(BAr$^{F}$) comprises one-quarter of both the thallium cation and the BAr$^{F}$ anion (see Fig. 1). The Tl atom lies directly on two of the fourfold axes of the unit cell, which also represent the axes along which anharmonic motion occurs (see Fig. S7). Additionally, the B atoms occupy the two remaining $C_4$ axes. Therefore, the BAr$^{F}$ anion exhibits $S_4$ symmetry. The tetrahedral coordination environment of the B atoms is slightly distorted, as indicated by the C1—B1—C1$^{iv}$ angle of 109.71 (5)° [symmetry code: (iv) $y+\frac{1}{2}, -x+1, -z+2$], which deviates from the angle of 109.5° in an idealized tetrahedron.

There are three distinct correlated positions of the arene rings, tilted by 5.49 and 6.15° (see Fig. S5), with the three components refining to occupancies of 0.579 (7), 0.263 (7) and 0.158 (5). This disorder is directly connected to a supra-

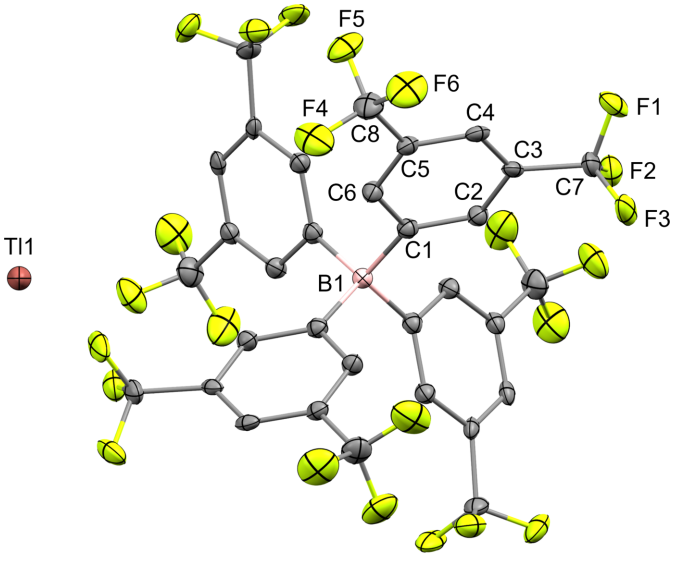


**Figure 1**
The structure of Tl(BAr$^{F}$), as determined by SC-XRD, with the atom-numbering scheme, viewed along the $c$ axis. For clarity, the figure only shows PART 1, with only the atoms of the asymmetric unit labelled and H atoms omitted. Atoms H2, H4 and H6 are attached to the C atoms with the same numbers. All displacement ellipsoids are drawn at the 50% probability level.

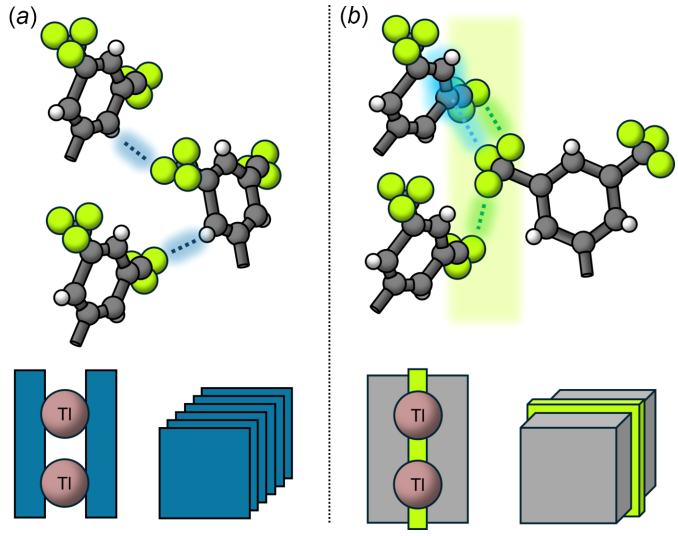


**Figure 2**
Schematic representation of the hinge-like interactions between the BAr$^{F}$ anions. (*a*) In the part with major occupancy, layers of nonclassical hydrogen bonds form a herringbone pattern along the *a* and *b* axes, and a stacking motif along the *c* axis, with the thallium ions in between (bottom left). (*b*) C—F···$\pi$ and F···F contacts in the minor components form 'fluorous' interlayers along the *a* and *b* axes and a barrier-like layer along the *c* axis (bottom right).

molecular feature of the structure, giving rise to two domains in which different intermolecular fluorine-based interactions dominate (see Fig. 2 and Table 2). The major component (PART 1) is associated with a network of weak nonclassical C—H···F hydrogen bonds, whereas the minor components (PART 2 and PART 3) are characterized by short F···F interactions and weak C—F···$\pi$ interactions. Generally, the co-existence of both nonclassical C—H···F hydrogen bonds and F···F interactions with dispersive character within the same structure, while simultaneously leading to self-sorting, is not uncommon in fluorine-rich organic molecules (Pickl *et al.*, 2024). Overall, the structure of Tl(BAr$^{F}$) displays hinge-like supramolecular interactions between the BAr$^{F}$ anions, held together by comparatively weak intermolecular interactions. In the part with major occupancy, a weak but directional C—H···F interaction between H6 and F1$^{ii}$ (Table 2) is present, suggesting a nonclassical hydrogen bond, with the H6···F1$^{ii}$ distance of 2.621 (7) Å being slightly shorter than the sum of the van der Waals radii. Due to the $S_4$ symmetrical nature of the BAr$^{F}$ anion, this leads to a herringbone-type arrangement of C—H···F interactions, which produces layers along the *ab* plane. A similar network of nonclassical hydrogen bonds is missing in the two minor-occupancy regions, as deduced from the corresponding H6$A$···F1$A^{ii}$ [2.868 (14) Å] and H6$B$···F1$B^{ii}$ [2.856 (17) Å] distances. Instead, there are short but weak C—F···$\pi$ contacts (see Table 2) between F atoms and adjacent aromatic rings. The geometry, with approximately perpendicular ring planes and an $\eta^2$-like interaction motif, suggests weak but directed C—F···$\pi$ interactions. Specifically for PART 2, there is also a short F3$A$···F4$A^{i}$ contact (Table 2) of 2.90 (3) Å between the $CF_3$

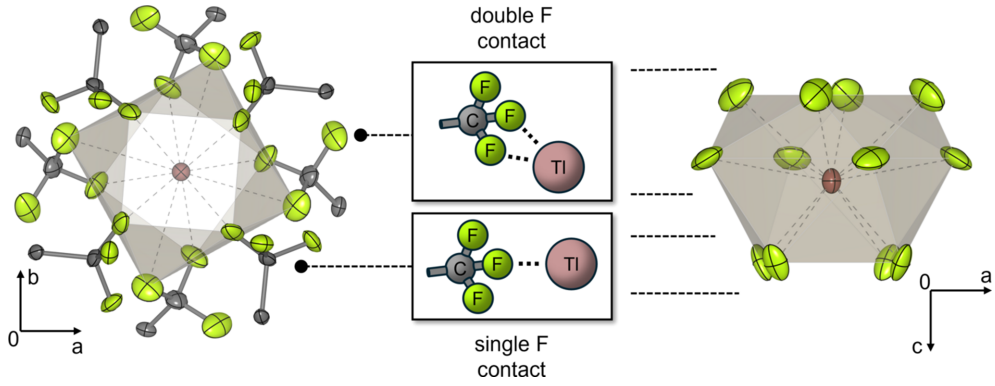


**Figure 3**
Distorted cuboctahedral pseudo-coordination polyhedron around the central Tl atom, either viewed along the *c* axis (left) or the *b* axis (right), with displacement ellipsoids drawn at the 50% probability level. The $CF_3$ groups interact with the Tl atom *via* either two F atoms as a double contact or *via* one F atom as a single contact.

groups of the anions. In the two parts with minor occupancy, these short C—F···$\pi$ and F···F contacts form a 'fluorous' interlayer around the Tl atoms; the interlayer lies parallel to the *a* and *b* axes, but perpendicular to the *c* axis. Therefore, the rings of the $BAr^F$ anions either twist against each other in the part with major occupancy to form nonclassical hydrogen-bond networks, or the rings tilt towards each other in the two parts with minor occupancy to form an interlayer of short F···F, as well as weak $\eta^2$-like C—F···$\pi$ contacts (see Fig. S6). This structural flexibility is somewhat reminiscent of the 'breathing' described for soft crystalline materials (Horike *et al.*, 2009), although in the presented structure, no discrete open and closed states at the microscale or phase transitions at the macroscale are observed.

**Table 3**
Close Tl···F contacts (Å), as identified by *PLATON* (Spek, 2020).

| | | | |
|---|---|---|---|
| Tl1···F3 | 2.896 (7) | Tl1···F4*A*$^{i}$ | 3.15 (2) |
| Tl1···F5$^{i}$ | 3.050 (4) | Tl1···F6*A*$^{i}$ | 3.233 (9) |
| Tl1···F6$^{i}$ | 3.191 (12) | Tl1···F3*B* | 3.070 (12) |
| Tl1···F3*A* | 2.824 (16) | Tl1···F4*B*$^{i}$ | 3.01 (3) |

Symmetry code: (i) $-x+1, -y+1, -z+1$.

Besides supramolecular networks and layered structures, close Tl···F contacts within the range 2.824 (16)–3.233 (9) Å were detected (see Table 3), rendering $Tl(BAr^F)$ a contact ion pair. Such contacts have also been reported for other thallium salts of weakly coordinating anions (Hughes *et al.*, 1997; Parvez *et al.*, 2005). The distances described in this work are among the shortest yet. In $Tl(BAr^F)\cdot 0.33CH_2Cl_2$, the Tl···F distances within the sum of the van der Waals radii are 3.05 (6) and 3.18 (6) Å (Hughes *et al.*, 1997), while the distances in $Tl[B(C_6F_5)_4]$ lie between 2.942 (4) and 3.663 (4) Å (Parvez *et al.*, 2005). For comparison, in thallium(I) fluoride, the interatomic Tl—F distances within the sum of the van der Waals radii (including actual covalent bonds) range from 2.251 (17) to 3.496 (14) Å (Alcock & Jenkins, 1974). Despite such close contacts in solvent-free $Tl(BAr^F)$, the C—F bond lengths seem to be largely unaffected, since they are in a reasonable range between 1.335 (4) and 1.366 (7) Å for the part with major occupancy, for which the C—F distances were allowed to refine freely. Overall, each Tl atom is surrounded by 12 F atoms, resulting in a cuboctahedral pseudo-coordination polyhedron. The coordination environment is strongly distorted, as indicated by the differing range of Tl···F contact

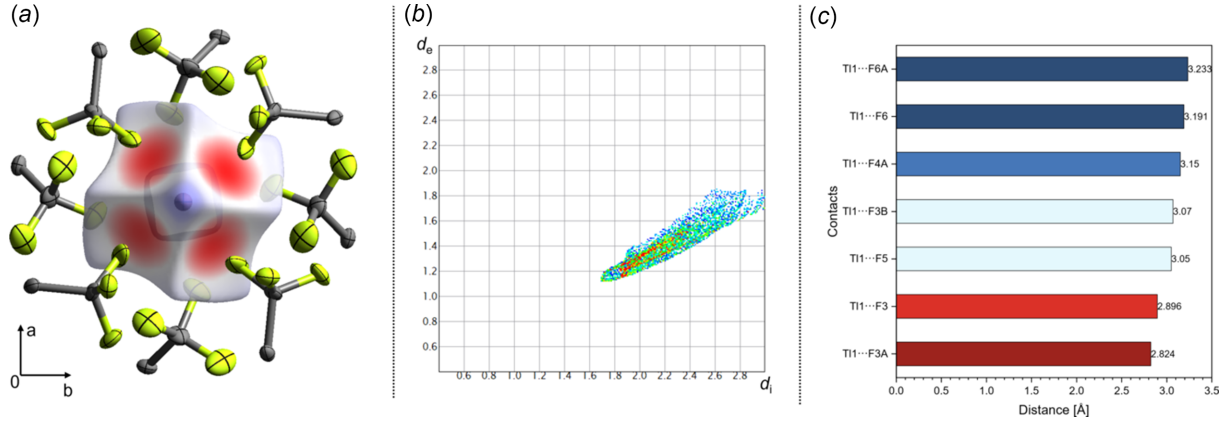


**Figure 4**
(*a*) Hirshfeld surface of Tl1, generated with *CrystalExplorer*, indicating short Tl···F contacts as bright red spots on the surface representation, as viewed along the *c* axis. (*b*) The fingerprint plot of $d_e$ over $d_i$ shows only Tl···F interactions. (*c*) Histogram plot of the differing Tl···F contact distances, revealing Tl1···F3*A* and Tl1···F3 as the shortest contacts (red bars).

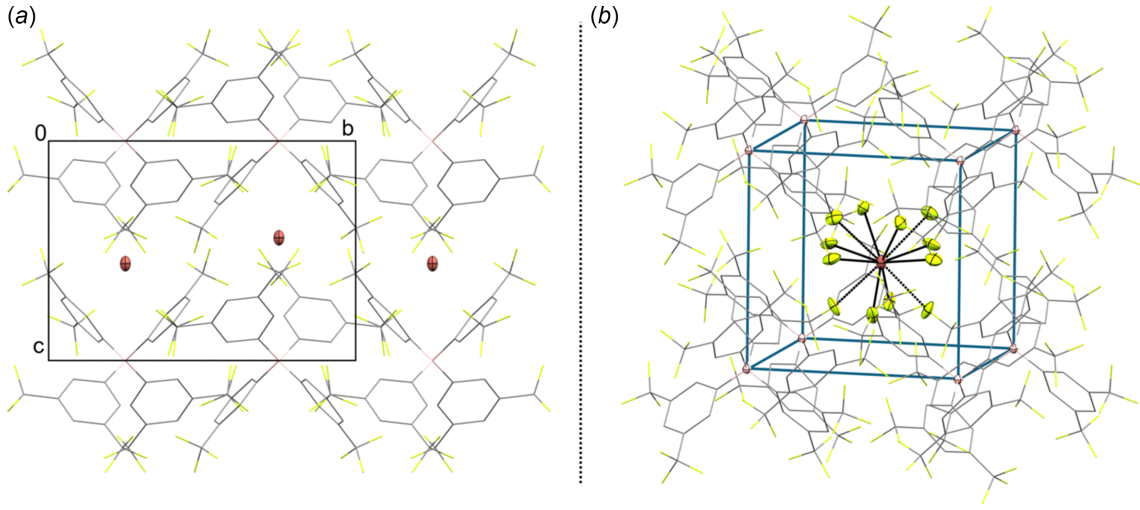


**Figure 5**
(*a*) Packing diagram of Tl(BAr$^F$), viewed along the *a* axis, showing a zigzag alignment of Tl atoms. (*b*) The expanded unit cell exhibits a virtually cubic arrangement of eight BAr$^F$ anions around the central Tl atom. Tl atoms, as well as B atoms and short-contact F atoms in part (*b*), are displayed as displacement ellipsoids at the 50% probability level; the remaining atoms are displayed in wireframe mode.

distances between 2.824 (16) and 3.233 (9) Å, as well as the view along the crystallographic *b* axis (see Fig. 3). This is a consequence of the $CF_3$ moieties of the BAr$^F$ anions interacting with the Tl atom, either with two F atoms or only one at the basis of the cuboctahedron.

Hirshfeld surface analysis of Tl1, using *CrystalExplorer* (Spackman *et al.*, 2021), confirms Tl···F contacts as the sole interactions for the Tl atoms with the surrounding anions. The Hirshfeld surface mapped over $d_{norm}$ for the part with major occupancy revealed several short Tl···F contacts as bright red spots in the graphical representation [see Fig. 4(*a*)]. The two-dimensional fingerprint plot of $d_e$ over $d_i$ [the distances to the nearest atom internal or external to the surface; Fig. 4(*b*)] shows that these contacts are indeed the only interactions between the thallium cations and the BAr$^F$ anions, accounting for 100% of the total surface area.

Tl···F contacts, forming a distorted coordination environment around Tl, also affect the packing of Tl(BAr$^F$). Alternating units of Tl···F cuboctahedra lead to a zigzag motif of thallium cations, which is clearly visible along the crystallographic *a* axis [see Fig. 5(*a*)]. In the expanded unit cell, eight BAr$^F$ anions surround one Tl atom, which results in a cage-like nearly cubic arrangement of BAr$^F$ anions, with isolated Tl centres showing no Tl···Tl contacts [see Fig. 5(*b*)]. This matches well with previous reports on alkali-metal BAr$^F$ salts, such as anhydrous and solvent-free Na(BAr$^F$) (CCDC 1886446) and K(BAr$^F$) (CCDC 1886447) (Martínez-Martínez & Weller, 2019), which also exhibit a virtually cubic arrangement of the weakly coordinating anions. The effective pseudo-coordination number in these salts is 8, whereas it is 12 in Tl(BAr$^F$), most probably due to the larger radius of the Tl$^I$ cation.

To confirm that the bulk of Tl(BAr$^F$) has the same (solvent-free) structure as derived from SC-XRD, we performed PXRD measurements of the obtained material. The diffractogram, acquired at room temperature rather than at 100 K as in the SC-XRD measurement, matches well with its SC-XRD counterpart (see Figs. 6 and S8). The indexed unit cell exhibits primitive tetragonal symmetry, suggesting a largely similar structure to that at 100 K. Interestingly, comparing the unit cells at 100 K and at room temperature reveals anisotropic elongation along the crystallographic *a* and *b* axes. Both axes expand to 13.859 (7) Å, which corresponds to an increase by 2.7%. In contrast, the *c* axis remains nearly unchanged with a length of 9.675 (7) Å, which corresponds to a comparably small expansion by 0.5%. This is also reflected in the overlay of the low-temperature structure with the simulated room-temperature structure [see Fig. 6(*b*)]. The view along the *b* axis shows virtually no expansion for the unit cell along the *c* axis but pronounced expansion along the *a* and *b* axes, which is also clearly visible in the view along the *c*-axes of the overlay. This thermal expansion behaviour may tentatively correlate with the supramolecular networks that produce layer-like structures in both components of the disorder. In the part with major occupancy, the herringbone arrangement of nonclassical hydrogen bonds forms layers along the *ab* plane, which are perpendicular to the *c* axis. In the minor parts of the structure, short C—F···$\pi$ and F···F contacts form a 'fluorous' interlayer around the Tl atoms, which also lies parallel to the *a* and *b* axes, but perpendicular to the *c* axis. While these two types of layers lie in the same direction within the unit cell and can 'glide' comparably easily against each other along the *a* and *b* axes, we assume that the *c* axis appears to be more 'locked', with the networks perpendicular to it. This presumably reduces flexibility along the *c* axis and allows for easier movement of the structure along the *a* and *b* axes.

In addition, TGA of the obtained Tl(BAr$^F$) under an argon atmosphere (see Fig. 7) shows that the bulk material is solvent-free, as anticipated from the SC-XRD structure. No mass loss is observed until an onset temperature of 245 °C, which marks the decomposition point of Tl(BAr$^F$). At its first decomposition step, the sample of Tl(BAr$^F$) loses 59.46% of

weight, which corresponds to the loss of the borane $B[C_6H_3(CF_3)_2]_3$ ($M$ = 650.12 g mol$^{-1}$; 60.90%) from the $BAr^F$ borate anion. The peak temperature of this decomposition is 266 °C, as determined from the derivative thermogravimetry (DTG) plot, *i.e.* the first derivative of the TGA curve. The presumably remaining $TlC_6H_3(CF_3)_2$ species decomposes over a wider temperature range, eventually converging to a residual mass of 0 mg. This is most likely due to the formation of volatile TlF, which has a boiling point of 655 °C (Perry & Phillips, 1995), causing it to evaporate under these conditions. Similar thermal properties and decomposition temperatures have also been reported for systems containing structurally related borate anions, such as $[B(C_6F_5)_4]^-$ in imidazolium-based structures (Zhang *et al.*, 2012) or $Na[B\{C_6H_3(SF_5)_2\}_4]$ (Langford *et al.*, 2019).

## 4. Conclusion

In summary, the crystal structure of truly solvent-free $Tl(BAr^F)$ is presented. The structure comprises among the shortest Tl···F contacts reported to date, which represent the

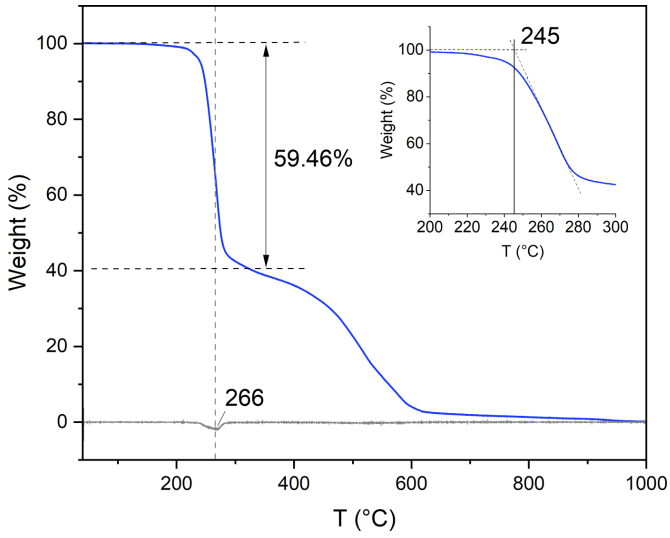


**Figure 7**
TGA (blue) and DTG (grey, bottom) curves of solvent-free $Tl(BAr^F)$ between 30 and 1000 °C at a heating rate of 2 °C min$^{-1}$ under an argon atmosphere with a flow rate of 25 ml min$^{-1}$. Decomposition occurs at 245 °C (see zoom-in), with a peak temperature of 266 °C.

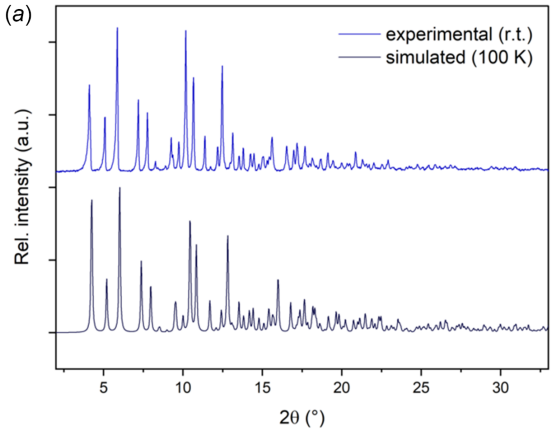


| | a, b [Å] | c [Å] |
|---|---|---|
| 100 K (SC-XRD) | 13.4930(4) | 9.6227(5) |
| Room temperature | 13.859(7) | 9.675(7) |
| **Expansion** | 2.7% | 0.5% |

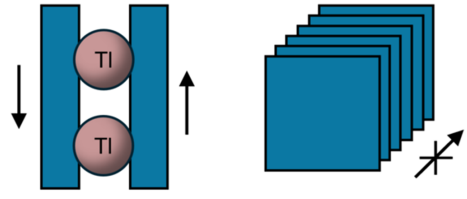


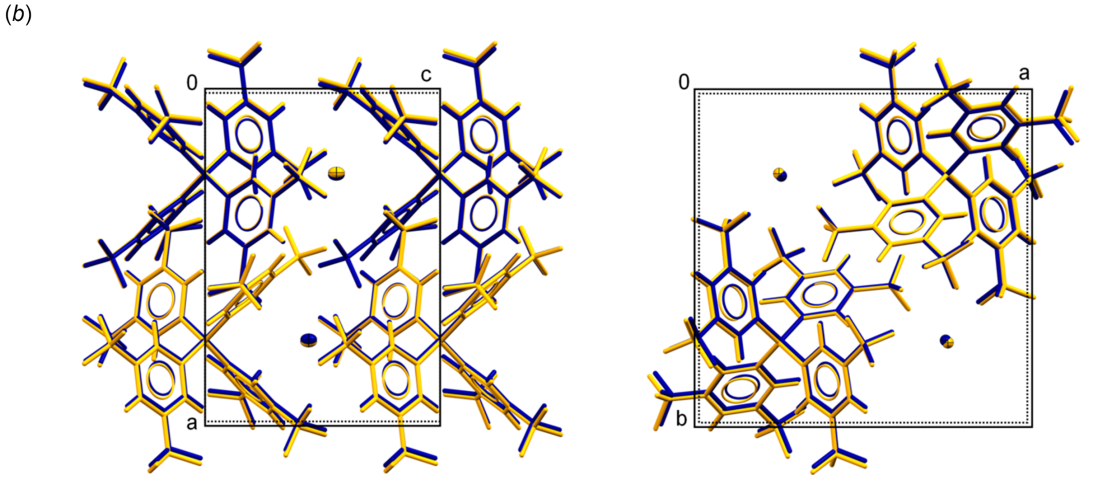


**Figure 6**
(*a*) Comparison of the powder X-ray diffractogram of $Tl(BAr^F)$ recorded at room temperature (top left trace, blue) and its simulated diffractogram based on the SC-XRD structure at 100 K (bottom left trace, dark blue). Anisotropic thermal expansion occurs along the *a* and *b* axes, with layers 'gliding' against each other along *a* and *b*, while the *c* axis does not expand significantly because both layer-like arrangements within the structure are perpendicular to it. (*b*) Overlay of the SC-XRD structure at 100 K (dark blue, dotted unit-cell box) and the simulated room-temperature structure (orange, solid unit-cell box), as viewed along the *b* axis (bottom left) and the *c* axis (bottom right).

primary direct interaction between the thallium cation and the $BAr^F$ anion. The compound exhibits a complex supramolecular organization characterized by hinge-like anion–anion interactions that are closely associated with disorder of the aryl rings. This gives rise to a herringbone arrangement of nonclassical C—H···F hydrogen bonds in the major disorder component, while the minor components form 'fluorous' interlayers dominated by C—F···$\pi$ and F···F contacts. These supramolecular features correlate with anisotropic thermal expansion of the unit-cell parameters along the *a* and *b* axes, as determined by variable-temperature PXRD measurements. In addition, PXRD and TGA analyses confirm that the bulk material is phase-pure and retains the solvent-free structure observed by SC-XRD.

## Acknowledgements

This work was funded by the German Research Foundation (DFG) and the TUM Graduate School. The authors thank Professor Roland A. Fischer (TUM) and the Technical University of Munich (Catalysis Research Center) for financial support and laboratory equipment, and Dr Wilhelm Klein (TUM & Catalysis Research Center) for help with analysing PXRD data. Open access funding enabled and organized by Projekt DEAL.

## Funding information

Funding for this research was provided by: German Research Foundation (grant No. FI-502/44-1); TUM Graduate School.

## References

Alberti, D. & Pörschke, K.-R. (2004). *Organometallics* **23**, 1459–1460.
Alcock, N. W. & Jenkins, H. D. B. (1974). *J. Chem. Soc. Dalton Trans.* pp. 1907–1911.
Allen, F. H., Johnson, O., Shields, G. P., Smith, B. R. & Towler, M. (2004). *J. Appl. Cryst.* **37**, 335–338.
Bourhis, L. J., Dolomanov, O. V., Gildea, R. J., Howard, J. A. K. & Puschmann, H. (2015). *Acta Cryst.* A**71**, 59–75.
Bruker (2014). *XPREP*. Bruker AXS Inc., Madison, Wisconsin, USA.
Bruker (2016). *SADABS*. Bruker AXS Inc., Madison, Wisconsin, USA.
Bruker (2019). *SAINT*. Bruker AXS Inc., Madison, Wisconsin, USA.
Bruker (2022). *APEX4*. Bruker AXS Inc., Madison, Wisconsin, USA.
Carreras, L., Rovira, L., Vaquero, M., Mon, I., Martin, E., Benet-Buchholz, J. & Vidal-Ferran, A. (2017). *RSC Adv.* **7**, 32833–32841.
Dolomanov, O. V., Bourhis, L. J., Gildea, R. J., Howard, J. A. K. & Puschmann, H. (2009). *J. Appl. Cryst.* **42**, 339–341.
Evans, D. R., Drovetskaya, T., Bau, R., Reed, C. A. & Boyd, P. D. W. (1997). *J. Am. Chem. Soc.* **119**, 3633–3634.
Flack, H. D. (1983). *Acta Cryst.* A**39**, 876–881.
He, T., Bruening, M. A., Espinosa, M. & Agapie, T. (2025). *Angew. Chem. Int. Ed.* **64**, e202417136.
Heintz, R. A., Smith, J. A., Szalay, P. S., Weisgerber, A. & Dunbar, K. R. (2002). *Inorganic Syntheses*, edited by D. Coucouvanis, pp. 75–121. Hoboken, New Jersey: John Wiley & Sons, Inc.
Horike, S., Shimomura, S. & Kitagawa, S. (2009). *Nat. Chem.* **1**, 695–704.
Hübschle, C. B., Sheldrick, G. M. & Dittrich, B. (2011). *J. Appl. Cryst.* **44**, 1281–1284.
Hughes, R. P., Lindner, D. C., Rheingold, A. L. & Yap, G. P. A. (1997). *Inorg. Chem.* **36**, 1726–1727.
Kelling, L., Esser, J., Knyszek, D. & Gessner, V. H. (2024). *Angew. Chem. Int. Ed.* **63**, e202405936.
Kim, K.-C., Reed, C. A., Elliott, D. W., Mueller, L. J., Tham, F., Lin, L. & Lambert, J. B. (2002). *Science* **297**, 825–827.
Kratzert, D. (2026). *FinalCif*. https://dkratzert.de/finalcif.html.
Krossing, I. (2001). *Chem. Eur. J.* **7**, 490–502.
Krossing, I. & Raabe, I. (2004). *Angew. Chem. Int. Ed.* **43**, 2066–2090.
Kuhs, W. (1988). *Aust. J. Phys.* **41**, 369–382.
Lambert, J. B. & Zhang, S. (1993). *J. Chem. Soc. Chem. Commun.* pp. 383–384.
Langford, D., Göttker-Schnetmann, I., Wimmer, F. P., Casper, L. A., Kenyon, P., Winter, R. F. & Mecking, S. (2019). *Organometallics* **38**, 2710–2713.
Macrae, C. F., Sovago, I., Cottrell, S. J., Galek, P. T. A., McCabe, P., Pidcock, E., Platings, M., Shields, G. P., Stevens, J. S., Towler, M. & Wood, P. A. (2020). *J. Appl. Cryst.* **53**, 226–235.
Martínez-Martínez, A. J. & Weller, A. S. (2019). *Dalton Trans.* **48**, 3551–3554.
Massey, A. G. & Park, A. J. (1964). *J. Organomet. Chem.* **2**, 245–250.
McSkimming, A. (2025). *Organometallics* **44**, 1630–1632.
Momma, K. & Izumi, F. (2011). *J. Appl. Cryst.* **44**, 1272–1276.
Nishida, H., Takada, N., Yoshimura, M., Sonoda, T. & Kobayashi, H. (1984). *Bull. Chem. Soc. Jpn* **57**, 2600–2604.
Parvez, M., Piers, W. E. & Ghesner, I. (2005). *Acta Cryst.* E**61**, m1801–m1803.
Perry, D. L. & Phillips, S. L. (1995). *Handbook of Inorganic Compounds*, p. 407. Boca Raton: CRC Press.
Pickl, T., Zuber, J., Stephan, J. & Pöthig, A. (2024). *Acta Cryst.* C**80**, 278–283.
Pike, S. D., Thompson, A. L., Algarra, A. G., Apperley, D. C., Macgregor, S. A. & Weller, A. S. (2012). *Science* **337**, 1648–1651.
Reed, C. A. (1998). *Acc. Chem. Res.* **31**, 133–139.
Riddlestone, I. M., Kraft, A., Schaefer, J. & Krossing, I. (2018). *Angew. Chem. Int. Ed.* **57**, 13982–14024.
Salem, H., Shimon, L. J. W., Leitus, G., Weiner, L. & Milstein, D. (2008). *Organometallics* **27**, 2293–2299.
Scholz, F., Himmel, D., Heinemann, F. W., Schleyer, P., v, R., Meyer, K. & Krossing, I. (2013). *Science* **341**, 62–64.
Seidel, S. & Seppelt, K. (2000). *Science* **290**, 117–118.
Sheldrick, G. M. (2015*a*). *Acta Cryst.* A**71**, 3–8.
Sheldrick, G. M. (2015*b*). *Acta Cryst.* C**71**, 3–8.
Spackman, P. R., Turner, M. J., McKinnon, J. J., Wolff, S. K., Grimwood, D. J., Jayatilaka, D. & Spackman, M. A. (2021). *J. Appl. Cryst.* **54**, 1006–1011.
Spek, A. L. (2020). *Acta Cryst.* E**76**, 1–11.
Stephan, J., Bühler, R., Napoli, F. E., Gemel, C. & Fischer, R. A. (2025). *Inorg. Chem.* **64**, 15707–15714.
Zhang, B., Köberl, M., Pöthig, A., Cokoja, M., Herrmann, W. A. & Kühn, F. E. (2012). *Z. Naturforsch. B* **67**, 1030–1036.

# supporting information

*Acta Cryst.* (2026). C**82** [https://doi.org/10.1107/S2053229626008454]

## Solvent-free thallium(I) tetrakis[3,5-bis(trifluoromethyl)phenyl]borate: crystal structure, supramolecular interactions and anisotropic thermal expansion

**Johannes Stephan, Lena Schröck, E. Eja Petersen, Romy L. Ettlinger and Alexander Pöthig**

### Computing details

#### Thallium(I) tetrakis[3,5-bis(trifluoromethyl)phenyl]borate

*Crystal data*

$Tl^{+}\cdot C_{32}H_{12}BF_{24}^{-}$
$M_r$ = 1067.63
Tetragonal, $P4/n$
$a$ = 13.4930 (4) Å
$c$ = 9.6227 (5) Å
$V$ = 1751.92 (12) Å$^3$
$Z$ = 2
$F(000)$ = 1011.963
$D_x$ = 2.024 Mg m$^{-3}$
Mo $K\alpha$ radiation, $\lambda$ = 0.71073 Å
Cell parameters from 9110 reflections
$\theta$ = 2.6–30.4°
$\mu$ = 4.76 mm$^{-1}$
$T$ = 100 K
Block, colourless
0.16 × 0.15 × 0.10 mm

*Data collection*

Bruker D8 VENTURE diffractometer
Radiation source: TXS rotating anode
Helios optic monochromator
Detector resolution: 16 pixels mm$^{-1}$
$\omega$ and $\varphi$ scans
Absorption correction: multi-scan (SADABS; Bruker, 2016)
$T_{min}$ = 0.633, $T_{max}$ = 0.747
87174 measured reflections
3197 independent reflections
2970 reflections with $I \geq 2u(I)$
$R_{int}$ = 0.055
$\theta_{max}$ = 32.6°, $\theta_{min}$ = 2.1°
$h$ = −20→20
$k$ = −19→20
$l$ = −14→14

*Refinement*

Refinement on $F^2$
Least-squares matrix: full
$R[F^2 > 2\sigma(F^2)]$ = 0.021
$wR(F^2)$ = 0.053
$S$ = 1.06
3197 reflections
284 parameters
697 restraints
31 constraints
Primary atom site location: iterative
Secondary atom site location: difference Fourier map
Hydrogen site location: inferred from neighbouring sites
H atoms treated by a mixture of independent and constrained refinement
$w = 1/[\sigma^2(F_o^2) + (0.0325P)^2 + 0.564P]$ where $P = (F_o^2 + 2F_c^2)/3$
$(\Delta/\sigma)_{max}$ = 0.0002
$\Delta\rho_{max}$ = 0.59 e Å$^{-3}$
$\Delta\rho_{min}$ = −0.86 e Å$^{-3}$

*Special details*

**Experimental**. Diffractometer operator Johannes Stephan scanspeed 1-3 s per frame dx 46 mm 2604 frames measured in 10 data sets phi-scans with delta_phi = 0.5 omega-scans with delta_omega = 0.5 shutterless mode

**Geometry**. Short intermolecular Tl···F contacts, a weak nonclassical C-H···F hydrogen bond, as well as short intermolecular C-F···$\pi$ and F···F contacts were identified in this structure by RTAB in SHELXL and Olex2 1.5-beta, and contact analysis in PLATON (Spek, 2020) using CALC GEOM. These interactions are not included in the formal bonding scheme since they involve multiple symmetry-equivalent images of the same physical contacts. Only the shortest unique symmetry representation has been included in the geometry table to avoid redundancy.
Short Tl···F contacts: Tl1···F3 = 2.896 (7) Å Tl1···F5 = 3.050 (4) Å Tl1···F6 = 3.191 (12) Å Tl1···F3A = 2.824 (16) Å Tl1···F4A = 3.15 (2) Å Tl1···F6A = 3.233 (9) Å Tl1···F3B = 3.070 (12) Å Tl1···F4B = 3.01 (3) Å
Weak, nonclassical C-H···F hydrogen bond: H6···F1 = 2.621 (7) Å
Short F···F contact: F3A···F4A = 2.90 (3) Å
Short C-F···$\pi$ contacts: F5A···C4A = 3.180 (9) Å F5A···C5A = 3.153 (8) Å F5B···C4B = 3.195 (12) Å F5B···C5B = 3.182 (12) Å

**Refinement**. Unit-cell determination and data integration and reduction were performed with *SAINT* (Bruker, 2019) and *SADABS* (Bruker, 2016), as implemented in the *APEX4* software package (Bruker, 2022). Space-group determination and solution were based on *SHELXT* (Sheldrick, 2015*a*), and refinement was performed with *SHELXL* (Sheldrick, 2015*b*) in conjunction with *ShelXle* (Hübschle, 2011).

*Fractional atomic coordinates and isotropic or equivalent isotropic displacement parameters (Å²)*

| | *x* | *y* | *z* | $U_{iso}$*/$U_{eq}$ | Occ. (<1) |
|---|---|---|---|---|---|
| Tl1 | 0.25 | 0.25 | 0.55897 (3) | 0.03005 (18) | |
| F1 | 0.3846 (6) | 0.5041 (5) | 0.7957 (5) | 0.0356 (9) | 0.579 (7) |
| F2 | 0.3889 (3) | 0.4067 (3) | 0.9793 (6) | 0.0337 (7) | 0.579 (7) |
| F3 | 0.3671 (7) | 0.3499 (7) | 0.7688 (7) | 0.0411 (8) | 0.579 (7) |
| F4 | 0.8196 (4) | 0.4522 (3) | 0.5553 (5) | 0.0544 (13) | 0.579 (7) |
| F5 | 0.7758 (3) | 0.5861 (3) | 0.6562 (4) | 0.0452 (8) | 0.579 (7) |
| F6 | 0.6848 (8) | 0.5254 (8) | 0.4909 (9) | 0.0522 (17) | 0.579 (7) |
| F1A | 0.3920 (13) | 0.5036 (10) | 0.8229 (17) | 0.0356 (9) | 0.263 (7) |
| F2A | 0.3860 (8) | 0.3834 (7) | 0.9567 (10) | 0.0337 (7) | 0.263 (7) |
| F3A | 0.3804 (13) | 0.3451 (14) | 0.746 (2) | 0.0411 (8) | 0.263 (7) |
| F4A | 0.6627 (14) | 0.5377 (14) | 0.4993 (18) | 0.036 (2) | 0.263 (7) |
| F5A | 0.7748 (8) | 0.4230 (6) | 0.5053 (9) | 0.0502 (19) | 0.263 (7) |
| F6A | 0.7894 (6) | 0.5525 (8) | 0.6231 (10) | 0.050 (2) | 0.263 (7) |
| F1B | 0.3896 (14) | 0.4891 (10) | 0.775 (2) | 0.0356 (9) | 0.158 (5) |
| F2B | 0.4013 (12) | 0.4230 (13) | 0.9654 (15) | 0.0337 (7) | 0.158 (5) |
| F3B | 0.3787 (12) | 0.3337 (9) | 0.7945 (18) | 0.0411 (8) | 0.158 (5) |
| F4B | 0.683 (3) | 0.5437 (17) | 0.513 (3) | 0.049 (4) | 0.158 (5) |
| F5B | 0.7332 (8) | 0.4046 (9) | 0.4564 (9) | 0.053 (3) | 0.158 (5) |
| F6B | 0.8277 (9) | 0.4847 (12) | 0.5853 (14) | 0.046 (3) | 0.158 (5) |
| C1 | 0.68301 (18) | 0.32269 (14) | 0.9011 (2) | 0.0163 (3) | 0.579 (7) |
| C2 | 0.5805 (3) | 0.3380 (3) | 0.9154 (4) | 0.0161 (8) | 0.579 (7) |
| H2 | 0.5443 (3) | 0.3027 (3) | 0.9841 (4) | 0.0194 (10)* | 0.579 (7) |
| C3 | 0.5312 (3) | 0.4061 (3) | 0.8273 (5) | 0.0198 (7) | 0.579 (7) |
| C4 | 0.5813 (3) | 0.4593 (3) | 0.7260 (5) | 0.0212 (6) | 0.579 (7) |
| H4 | 0.5470 (3) | 0.5053 (3) | 0.6687 (5) | 0.0255 (8)* | 0.579 (7) |
| C5 | 0.6824 (3) | 0.4440 (3) | 0.7096 (4) | 0.0217 (6) | 0.579 (7) |
| C6 | 0.7330 (3) | 0.3777 (3) | 0.7963 (4) | 0.0185 (6) | 0.579 (7) |
| H6 | 0.8024 (3) | 0.3693 (3) | 0.7848 (4) | 0.0222 (7)* | 0.579 (7) |

| | | | | | |
|---|---|---|---|---|---|
| C7 | 0.4186 (4) | 0.4172 (5) | 0.8463 (7) | 0.0251 (5) | 0.579 (7) |
| C8 | 0.7408 (3) | 0.5016 (3) | 0.6033 (5) | 0.0314 (7) | 0.579 (7) |
| C1A | 0.68301 (18) | 0.32269 (14) | 0.9011 (2) | 0.0163 (3) | 0.263 (7) |
| C2A | 0.5820 (3) | 0.3411 (3) | 0.9139 (4) | 0.0182 (17) | 0.263 (7) |
| H2A | 0.5490 (3) | 0.3109 (3) | 0.9901 (4) | 0.022 (2)* | 0.263 (7) |
| C3A | 0.5249 (5) | 0.3991 (5) | 0.8265 (7) | 0.0206 (14) | 0.263 (7) |
| C4A | 0.5691 (5) | 0.4491 (5) | 0.7168 (8) | 0.0216 (14) | 0.263 (7) |
| H4A | 0.5330 (5) | 0.4922 (5) | 0.6575 (8) | 0.0259 (17)* | 0.263 (7) |
| C5A | 0.6697 (5) | 0.4317 (4) | 0.6997 (6) | 0.0245 (14) | 0.263 (7) |
| C6A | 0.7243 (3) | 0.3682 (3) | 0.7843 (4) | 0.0205 (16) | 0.263 (7) |
| H6A | 0.7916 (3) | 0.3555 (3) | 0.7618 (4) | 0.0246 (19)* | 0.263 (7) |
| C7A | 0.4194 (7) | 0.4105 (8) | 0.8366 (11) | 0.0251 (5) | 0.263 (7) |
| C8A | 0.7214 (7) | 0.4845 (7) | 0.5837 (10) | 0.0314 (7) | 0.263 (7) |
| C1B | 0.6917 (9) | 0.3218 (6) | 0.8859 (10) | 0.0163 (3) | 0.158 (5) |
| C2B | 0.5936 (9) | 0.3384 (6) | 0.8985 (10) | 0.0196 (18) | 0.158 (5) |
| H2B | 0.5595 (9) | 0.3052 (6) | 0.9714 (10) | 0.023 (2)* | 0.158 (5) |
| C3B | 0.5399 (7) | 0.3988 (6) | 0.8152 (10) | 0.0207 (15) | 0.158 (5) |
| C4B | 0.5843 (6) | 0.4404 (6) | 0.7036 (9) | 0.0209 (15) | 0.158 (5) |
| H4B | 0.5478 (6) | 0.4782 (6) | 0.6379 (9) | 0.0251 (18)* | 0.158 (5) |
| C5B | 0.6830 (7) | 0.4257 (6) | 0.6899 (9) | 0.0227 (15) | 0.158 (5) |
| C6B | 0.7350 (8) | 0.3649 (6) | 0.7747 (10) | 0.0182 (18) | 0.158 (5) |
| H6B | 0.8030 (8) | 0.3524 (6) | 0.7558 (10) | 0.022 (2)* | 0.158 (5) |
| C7B | 0.4374 (9) | 0.4098 (9) | 0.8323 (14) | 0.0251 (5) | 0.158 (5) |
| C8B | 0.7334 (8) | 0.4666 (8) | 0.5684 (12) | 0.0314 (7) | 0.158 (5) |
| B1 | 0.75 | 0.25 | 1 | 0.0161 (4) | |

*Atomic displacement parameters (Å²)*

| | $U^{11}$ | $U^{22}$ | $U^{33}$ | $U^{12}$ | $U^{13}$ | $U^{23}$ |
|---|---|---|---|---|---|---|
| Tl1 | 0.02209 (17) | 0.02209 (17) | 0.0460 (3) | 0 | 0 | 0 |
| F1 | 0.0350 (11) | 0.0272 (9) | 0.045 (3) | 0.0156 (8) | −0.0119 (14) | −0.0032 (14) |
| F2 | 0.0220 (10) | 0.041 (3) | 0.0381 (14) | 0.0021 (13) | 0.0008 (8) | −0.0024 (9) |
| F3 | 0.022 (2) | 0.0374 (12) | 0.064 (3) | 0.0058 (15) | −0.0194 (13) | −0.0197 (14) |
| F4 | 0.066 (2) | 0.049 (2) | 0.049 (2) | 0.0089 (16) | 0.0279 (16) | 0.0203 (15) |
| F5 | 0.0541 (15) | 0.0375 (16) | 0.0439 (16) | −0.0190 (11) | −0.0013 (11) | 0.0120 (11) |
| F6 | 0.068 (4) | 0.057 (4) | 0.031 (2) | −0.007 (2) | −0.0052 (18) | 0.0181 (18) |
| F1A | 0.0350 (11) | 0.0272 (9) | 0.045 (3) | 0.0156 (8) | −0.0119 (14) | −0.0032 (14) |
| F2A | 0.0220 (10) | 0.041 (3) | 0.0381 (14) | 0.0021 (13) | 0.0008 (8) | −0.0024 (9) |
| F3A | 0.022 (2) | 0.0374 (12) | 0.064 (3) | 0.0058 (15) | −0.0194 (13) | −0.0197 (14) |
| F4A | 0.051 (5) | 0.032 (4) | 0.024 (3) | 0.003 (3) | −0.004 (3) | 0.010 (2) |
| F5A | 0.062 (4) | 0.049 (3) | 0.040 (4) | 0.013 (3) | 0.023 (3) | 0.016 (2) |
| F6A | 0.046 (3) | 0.055 (5) | 0.049 (4) | −0.026 (3) | −0.003 (2) | 0.021 (3) |
| F1B | 0.0350 (11) | 0.0272 (9) | 0.045 (3) | 0.0156 (8) | −0.0119 (14) | −0.0032 (14) |
| F2B | 0.0220 (10) | 0.041 (3) | 0.0381 (14) | 0.0021 (13) | 0.0008 (8) | −0.0024 (9) |
| F3B | 0.022 (2) | 0.0374 (12) | 0.064 (3) | 0.0058 (15) | −0.0194 (13) | −0.0197 (14) |
| F4B | 0.069 (9) | 0.039 (6) | 0.039 (8) | −0.001 (5) | 0.004 (5) | 0.027 (4) |
| F5B | 0.041 (5) | 0.090 (7) | 0.027 (4) | −0.011 (4) | 0.003 (3) | 0.008 (3) |
| F6B | 0.041 (4) | 0.063 (7) | 0.036 (4) | −0.035 (4) | −0.003 (3) | 0.014 (4) |

| | | | | | | |
|---|---|---|---|---|---|---|
| C1 | 0.0170 (7) | 0.0166 (5) | 0.0153 (6) | −0.0012 (4) | 0.0001 (5) | −0.0001 (4) |
| C2 | 0.0141 (14) | 0.0167 (15) | 0.0177 (15) | −0.0006 (8) | −0.0010 (8) | 0.0001 (8) |
| C3 | 0.0188 (12) | 0.0166 (12) | 0.0241 (14) | 0.0019 (7) | −0.0074 (7) | −0.0030 (8) |
| C4 | 0.0286 (12) | 0.0151 (12) | 0.0200 (12) | 0.0002 (8) | −0.0089 (8) | −0.0017 (8) |
| C5 | 0.0287 (12) | 0.0158 (11) | 0.0205 (11) | −0.0034 (8) | −0.0006 (7) | 0.0016 (8) |
| C6 | 0.0212 (12) | 0.0179 (11) | 0.0164 (12) | −0.0021 (7) | −0.0006 (8) | −0.0010 (8) |
| C7 | 0.0170 (10) | 0.0231 (9) | 0.0352 (11) | 0.0053 (7) | −0.0078 (7) | −0.0034 (7) |
| C8 | 0.0360 (16) | 0.0267 (17) | 0.0315 (14) | −0.0043 (10) | 0.0008 (10) | 0.0107 (10) |
| C1A | 0.0170 (7) | 0.0166 (5) | 0.0153 (6) | −0.0012 (4) | 0.0001 (5) | −0.0001 (4) |
| C2A | 0.018 (3) | 0.019 (3) | 0.018 (3) | −0.0018 (15) | −0.0004 (15) | −0.0013 (14) |
| C3A | 0.023 (2) | 0.018 (2) | 0.021 (2) | −0.0023 (12) | −0.0043 (12) | −0.0016 (12) |
| C4A | 0.024 (2) | 0.019 (2) | 0.021 (2) | −0.0002 (12) | −0.0070 (12) | −0.0020 (13) |
| C5A | 0.032 (2) | 0.021 (2) | 0.020 (2) | −0.0035 (12) | −0.0016 (12) | 0.0034 (13) |
| C6A | 0.021 (3) | 0.021 (3) | 0.020 (3) | −0.0029 (14) | −0.0007 (14) | −0.0018 (14) |
| C7A | 0.0170 (10) | 0.0231 (9) | 0.0352 (11) | 0.0053 (7) | −0.0078 (7) | −0.0034 (7) |
| C8A | 0.0360 (16) | 0.0267 (17) | 0.0315 (14) | −0.0043 (10) | 0.0008 (10) | 0.0107 (10) |
| C1B | 0.0170 (7) | 0.0166 (5) | 0.0153 (6) | −0.0012 (4) | 0.0001 (5) | −0.0001 (4) |
| C2B | 0.022 (3) | 0.019 (3) | 0.017 (3) | −0.0016 (15) | 0.0002 (16) | −0.0004 (15) |
| C3B | 0.018 (3) | 0.021 (3) | 0.024 (3) | 0.0000 (13) | −0.0054 (13) | −0.0019 (13) |
| C4B | 0.028 (3) | 0.018 (3) | 0.017 (3) | −0.0017 (13) | −0.0047 (13) | −0.0012 (14) |
| C5B | 0.027 (2) | 0.022 (3) | 0.019 (3) | −0.0031 (13) | −0.0010 (13) | 0.0020 (14) |
| C6B | 0.023 (3) | 0.019 (3) | 0.013 (3) | −0.0039 (15) | 0.0025 (15) | 0.0003 (15) |
| C7B | 0.0170 (10) | 0.0231 (9) | 0.0352 (11) | 0.0053 (7) | −0.0078 (7) | −0.0034 (7) |
| C8B | 0.0360 (16) | 0.0267 (17) | 0.0315 (14) | −0.0043 (10) | 0.0008 (10) | 0.0107 (10) |
| B1 | 0.0157 (7) | 0.0157 (7) | 0.0169 (12) | 0 | 0 | 0 |

*Geometric parameters (Å, º)*

| | | | |
|---|---|---|---|
| F1—C7 | 1.349 (7) | C5—C6 | 1.400 (4) |
| F2—C7 | 1.348 (7) | C5—C8 | 1.506 (4) |
| F3—C7 | 1.366 (7) | C6—H6 | 0.9500 |
| F4—C8 | 1.338 (6) | C1A—C2A | 1.391 (3) |
| F5—C8 | 1.335 (4) | C1A—C6A | 1.397 (3) |
| F6—C8 | 1.358 (9) | C1A—B1$^{i}$ | 1.638 (3) |
| F1A—C7A | 1.316 (13) | C2A—H2A | 0.9500 |
| F2A—C7A | 1.293 (12) | C2A—C3A | 1.383 (3) |
| F3A—C7A | 1.348 (13) | C3A—C4A | 1.388 (3) |
| F4A—C8A | 1.342 (12) | C3A—C7A | 1.435 (4) |
| F5A—C8A | 1.333 (10) | C4A—H4A | 0.9500 |
| F6A—C8A | 1.352 (9) | C4A—C5A | 1.387 (3) |
| F1B—C7B | 1.366 (14) | C5A—C6A | 1.392 (3) |
| F2B—C7B | 1.382 (14) | C5A—C8A | 1.498 (4) |
| F3B—C7B | 1.347 (13) | C6A—H6A | 0.9500 |
| F4B—C8B | 1.349 (16) | C1B—C2B | 1.349 (5) |
| F5B—C8B | 1.365 (12) | C1B—C6B | 1.351 (5) |
| F6B—C8B | 1.306 (13) | C1B—B1$^{i}$ | 1.662 (12) |
| C1—C2 | 1.405 (4) | C2B—H2B | 0.9500 |
| C1—C6 | 1.423 (4) | C2B—C3B | 1.354 (5) |

| | | | |
|---|---|---|---|
| C1—B1$^{i}$ | 1.638 (3) | C3B—C4B | 1.351 (5) |
| C2—H2 | 0.9500 | C3B—C7B | 1.401 (5) |
| C2—C3 | 1.416 (4) | C4B—H4B | 0.9500 |
| C3—C4 | 1.386 (4) | C4B—C5B | 1.353 (5) |
| C3—C7 | 1.538 (4) | C5B—C6B | 1.354 (5) |
| C4—H4 | 0.9500 | C5B—C8B | 1.460 (5) |
| C4—C5 | 1.390 (4) | C6B—H6B | 0.9500 |
| | | | |
| H6···F1$^{ii}$ | 2.621 (7) | Tl1···F6A$^{iii}$ | 3.233 (9) |
| Tl1···F3 | 2.896 (7) | Tl1···F3B | 3.070 (12) |
| Tl1···F5$^{iii}$ | 3.050 (4) | Tl1···F4B$^{iii}$ | 3.01 (3) |
| Tl1···F6$^{iii}$ | 3.191 (12) | F5A···C4A$^{iv}$ | 3.180 (9) |
| Tl1···F3A | 2.824 (16) | F5A···C5A$^{iv}$ | 3.153 (8) |
| Tl1···F4A$^{iii}$ | 3.15 (2) | F5B···C4B$^{iv}$ | 3.195 (12) |
| F3A···F4A$^{iii}$ | 2.90 (3) | F5B···C5B$^{iv}$ | 3.182 (12) |
| | | | |
| C6—C1—C2 | 117.3 (2) | F2B—C7B—F1B | 96.3 (13) |
| B1$^{i}$—C1—C2 | 125.05 (19) | F3B—C7B—F1B | 102.1 (11) |
| B1$^{i}$—C1—C6 | 117.57 (19) | F3B—C7B—F2B | 98.1 (12) |
| H2—C2—C1 | 120.02 (15) | C3B—C7B—F1B | 120.1 (10) |
| C3—C2—C1 | 120.0 (3) | C3B—C7B—F2B | 118.1 (10) |
| C3—C2—H2 | 120.02 (19) | C3B—C7B—F3B | 117.9 (10) |
| C4—C3—C2 | 121.9 (3) | F5B—C8B—F4B | 99.3 (16) |
| C7—C3—C2 | 117.2 (3) | F6B—C8B—F4B | 113.1 (19) |
| C7—C3—C4 | 121.0 (2) | F6B—C8B—F5B | 102.4 (11) |
| H4—C4—C3 | 120.59 (17) | C5B—C8B—F4B | 111.9 (17) |
| C5—C4—C3 | 118.8 (2) | C5B—C8B—F5B | 113.5 (7) |
| C5—C4—H4 | 120.59 (17) | C5B—C8B—F6B | 115.2 (9) |
| C6—C5—C4 | 120.3 (3) | C1$^{i}$—B1—C1 | 109.71 (5) |
| C8—C5—C4 | 120.9 (3) | C1$^{v}$—B1—C1$^{vi}$ | 109.71 (5) |
| C8—C5—C6 | 118.7 (3) | C1$^{v}$—B1—C1 | 109.71 (7) |
| C5—C6—C1 | 121.7 (3) | C1$^{i}$—B1—C1$^{v}$ | 108.99 (13) |
| H6—C6—C1 | 119.16 (15) | C1$^{vi}$—B1—C1 | 108.99 (13) |
| H6—C6—C5 | 119.16 (18) | C1$^{i}$—B1—C1$^{vi}$ | 109.71 (7) |
| F2—C7—F1 | 109.5 (5) | C1A—B1—C1 | 0.0 |
| F3—C7—F1 | 102.0 (6) | C1A$^{v}$—B1—C1$^{vi}$ | 109.71 (6) |
| F3—C7—F2 | 107.3 (5) | C1A$^{i}$—B1—C1$^{vi}$ | 109.71 (6) |
| C3—C7—F1 | 112.2 (5) | C1A—B1—C1$^{v}$ | 109.71 (6) |
| C3—C7—F2 | 113.3 (3) | C1A$^{v}$—B1—C1$^{i}$ | 108.99 (13) |
| C3—C7—F3 | 111.9 (5) | C1A—B1—C1$^{i}$ | 109.71 (6) |
| F5—C8—F4 | 106.0 (4) | C1A$^{i}$—B1—C1$^{i}$ | 0.0 |
| F6—C8—F4 | 106.5 (5) | C1A$^{vi}$—B1—C1 | 108.99 (13) |
| F6—C8—F5 | 107.4 (6) | C1A$^{v}$—B1—C1$^{v}$ | 0.0 |
| C5—C8—F4 | 113.2 (3) | C1A$^{vi}$—B1—C1$^{vi}$ | 0.0 |
| C5—C8—F5 | 111.5 (3) | C1A$^{i}$—B1—C1 | 109.71 (6) |
| C5—C8—F6 | 111.9 (6) | C1A$^{vi}$—B1—C1$^{v}$ | 109.71 (6) |
| C6A—C1A—C2A | 112.5 | C1A$^{i}$—B1—C1$^{v}$ | 108.99 (13) |
| B1$^{i}$—C1A—C2A | 126.6 | C1A$^{vi}$—B1—C1$^{i}$ | 109.71 (6) |

| | | | |
|---|---|---|---|
| B1$^{i}$—C1A—C6A | 120.7 | C1A$^{v}$—B1—C1 | 109.71 (6) |
| H2A—C2A—C1A | 116.82 (15) | C1A—B1—C1$^{vi}$ | 108.99 (13) |
| C3A—C2A—C1A | 126.4 | C1A$^{vi}$—B1—C1A | 108.99 (13) |
| C3A—C2A—H2A | 116.82 (15) | C1A$^{i}$—B1—C1A$^{v}$ | 108.99 (13) |
| C4A—C3A—C2A | 119.9 | C1A$^{i}$—B1—C1A | 109.71 (5) |
| C7A—C3A—C2A | 124.9 | C1A$^{v}$—B1—C1A | 109.71 (7) |
| C7A—C3A—C4A | 115.2 | C1A$^{v}$—B1—C1A$^{vi}$ | 109.71 (5) |
| H4A—C4A—C3A | 122.31 (14) | C1A$^{i}$—B1—C1A$^{vi}$ | 109.71 (7) |
| C5A—C4A—C3A | 115.4 | C1B—B1—C1 | 6.5 (4) |
| C5A—C4A—H4A | 122.31 (14) | C1B$^{v}$—B1—C1 | 115.0 (4) |
| C6A—C5A—C4A | 123.5 | C1B$^{i}$—B1—C1$^{vi}$ | 115.0 (4) |
| C8A—C5A—C4A | 117.6 | C1B—B1—C1$^{vi}$ | 103.1 (3) |
| C8A—C5A—C6A | 118.8 | C1B$^{v}$—B1—C1$^{i}$ | 103.1 (3) |
| C5A—C6A—C1A | 122.0 | C1B—B1—C1$^{v}$ | 110.2 (3) |
| H6A—C6A—C1A | 119.00 (14) | C1B$^{i}$—B1—C1$^{i}$ | 6.5 (4) |
| H6A—C6A—C5A | 119.00 (14) | C1B—B1—C1$^{i}$ | 115.0 (4) |
| F2A—C7A—F1A | 105.1 (12) | C1B$^{v}$—B1—C1$^{v}$ | 6.5 (4) |
| F3A—C7A—F1A | 116.7 (13) | C1B$^{vi}$—B1—C1 | 103.1 (3) |
| F3A—C7A—F2A | 105.0 (11) | C1B$^{i}$—B1—C1 | 110.2 (3) |
| C3A—C7A—F1A | 111.9 (9) | C1B$^{vi}$—B1—C1$^{vi}$ | 6.5 (4) |
| C3A—C7A—F2A | 112.1 (6) | C1B$^{i}$—B1—C1$^{v}$ | 103.1 (3) |
| C3A—C7A—F3A | 105.9 (9) | C1B$^{vi}$—B1—C1$^{v}$ | 115.0 (4) |
| F5A—C8A—F4A | 108.0 (10) | C1B$^{vi}$—B1—C1$^{i}$ | 110.2 (3) |
| F6A—C8A—F4A | 102.0 (12) | C1B$^{v}$—B1—C1$^{vi}$ | 110.2 (3) |
| F6A—C8A—F5A | 102.4 (9) | C1B—B1—C1A | 6.5 (4) |
| C5A—C8A—F4A | 115.5 (10) | C1B$^{vi}$—B1—C1A | 103.1 (3) |
| C5A—C8A—F5A | 112.2 (5) | C1B$^{i}$—B1—C1A$^{vi}$ | 115.0 (4) |
| C5A—C8A—F6A | 115.5 (6) | C1B—B1—C1A$^{vi}$ | 103.1 (3) |
| C6B—C1B—C2B | 115.1 | C1B$^{vi}$—B1—C1A$^{v}$ | 115.0 (4) |
| B1$^{i}$—C1B—C2B | 120.1 | C1B—B1—C1A$^{v}$ | 110.2 (3) |
| B1$^{i}$—C1B—C6B | 124.7 | C1B$^{i}$—B1—C1A$^{i}$ | 6.5 (4) |
| H2B—C2B—C1B | 117.6 (2) | C1B$^{v}$—B1—C1A | 115.0 (4) |
| C3B—C2B—C1B | 124.9 | C1B$^{vi}$—B1—C1A$^{vi}$ | 6.5 (4) |
| C3B—C2B—H2B | 117.6 (2) | C1B$^{v}$—B1—C1A$^{vi}$ | 110.2 (3) |
| C4B—C3B—C2B | 118.9 | C1B$^{i}$—B1—C1A | 110.2 (3) |
| C7B—C3B—C2B | 121.5 | C1B$^{v}$—B1—C1A$^{v}$ | 6.5 (4) |
| C7B—C3B—C4B | 119.1 | C1B$^{i}$—B1—C1A$^{v}$ | 103.1 (3) |
| H4B—C4B—C3B | 121.5 (2) | C1B$^{v}$—B1—C1A$^{i}$ | 103.1 (3) |
| C5B—C4B—C3B | 117.0 | C1B—B1—C1A$^{i}$ | 115.0 (4) |
| C5B—C4B—H4B | 121.5 (2) | C1B$^{vi}$—B1—C1A$^{i}$ | 110.2 (3) |
| C6B—C5B—C4B | 122.7 | C1B$^{i}$—B1—C1B$^{v}$ | 97.3 (6) |
| C8B—C5B—C4B | 118.8 | C1B$^{vi}$—B1—C1B | 97.3 (6) |
| C8B—C5B—C6B | 118.0 | C1B$^{i}$—B1—C1B | 115.9 (2) |
| C5B—C6B—C1B | 121.0 | C1B$^{v}$—B1—C1B | 115.9 (4) |
| H6B—C6B—C1B | 119.5 (2) | C1B$^{i}$—B1—C1B$^{vi}$ | 115.9 (4) |
| H6B—C6B—C5B | 119.5 (2) | C1B$^{v}$—B1—C1B$^{vi}$ | 115.9 (2) |
| | | | |
| F1—C7—C3—C2 | 158.6 (4) | C2—C1—B1—C1B | 154.8 (19) |

| | | | |
|---|---|---|---|
| F1—C7—C3—C4 | −22.8 (6) | C2—C3—C4—C5 | 0.9 (4) |
| F2—C7—C3—C2 | 34.0 (5) | C3—C2—C1—C6 | 0.0 (4) |
| F2—C7—C3—C4 | −147.4 (4) | C3—C2—C1—B1 | 177.2 (2) |
| F3—C7—C3—C2 | −87.5 (6) | C3—C4—C5—C6 | −1.4 (4) |
| F3—C7—C3—C4 | 91.1 (6) | C3—C4—C5—C8 | −178.5 (3) |
| F4—C8—C5—C4 | −151.4 (4) | C5—C4—C3—C7 | −177.7 (3) |
| F4—C8—C5—C6 | 31.5 (5) | C5—C6—C1—B1 | −178.0 (3) |
| F5—C8—C5—C4 | 89.3 (4) | C6—C1—B1—C1A$^{v}$ | 67.8 (3) |
| F5—C8—C5—C6 | −87.9 (4) | C6—C1—B1—C1A$^{vi}$ | −52.4 (3) |
| F6—C8—C5—C4 | −31.0 (6) | C6—C1—B1—C1A$^{i}$ | −172.5 (2) |
| F6—C8—C5—C6 | 151.8 (5) | C6—C1—B1—C1B$^{i}$ | −179.4 (5) |
| F1A—C7A—C3A—C2A | 135.6 (8) | C6—C1—B1—C1B$^{vi}$ | −55.1 (4) |
| F1A—C7A—C3A—C4A | −46.4 (10) | C6—C1—B1—C1B$^{v}$ | 71.9 (3) |
| F2A—C7A—C3A—C2A | 17.8 (10) | C6—C1—B1—C1B | −27.9 (19) |
| F2A—C7A—C3A—C4A | −164.3 (6) | C1A—C2A—C3A—C4A | −2.9 (4) |
| F3A—C7A—C3A—C2A | −96.2 (12) | C1A—C2A—C3A—C7A | 175.0 (4) |
| F3A—C7A—C3A—C4A | 81.8 (12) | C1A—C6A—C5A—C4A | −5.3 (4) |
| F4A—C8A—C5A—C4A | −5.5 (12) | C1A—C6A—C5A—C8A | 174.7 (4) |
| F4A—C8A—C5A—C6A | 174.5 (10) | C1A$^{vi}$—B1—C1A—C2A | 131.7 (2) |
| F5A—C8A—C5A—C4A | −129.9 (7) | C1A$^{i}$—B1—C1A—C2A | 11.5 (2) |
| F5A—C8A—C5A—C6A | 50.1 (7) | C1A$^{v}$—B1—C1A—C2A | −108.2 (2) |
| F6A—C8A—C5A—C4A | 113.3 (8) | C1A$^{i}$—B1—C1A—C6A | −163.6 (2) |
| F6A—C8A—C5A—C6A | −66.7 (8) | C1A$^{v}$—B1—C1A—C6A | 76.70 (19) |
| F1B—C7B—C3B—C2B | 162.2 (9) | C1A$^{vi}$—B1—C1A—C6A | −43.45 (19) |
| F1B—C7B—C3B—C4B | −25.4 (12) | C1A$^{v}$—B1—C1B—C2B | −109.5 (3) |
| F2B—C7B—C3B—C2B | 45.3 (12) | C1A$^{vi}$—B1—C1B—C2B | 133.5 (2) |
| F2B—C7B—C3B—C4B | −142.3 (10) | C1A$^{i}$—B1—C1B—C2B | 14.2 (3) |
| F3B—C7B—C3B—C2B | −72.3 (11) | C1A—B1—C1B—C2B | −23 (2) |
| F3B—C7B—C3B—C4B | 100.1 (11) | C1A$^{v}$—B1—C1B—C6B | 72.4 (3) |
| F4B—C8B—C5B—C4B | 23.3 (15) | C1A$^{vi}$—B1—C1B—C6B | −44.7 (3) |
| F4B—C8B—C5B—C6B | −164.4 (13) | C1A—B1—C1B—C6B | 159 (3) |
| F5B—C8B—C5B—C4B | −88.1 (9) | C1A$^{i}$—B1—C1B—C6B | −164.0 (3) |
| F5B—C8B—C5B—C6B | 84.2 (9) | C2A—C1A—C6A—C5A | 5.4 (3) |
| F6B—C8B—C5B—C4B | 154.3 (10) | C2A—C1A—B1—C1B$^{i}$ | 4.7 (5) |
| F6B—C8B—C5B—C6B | −33.4 (11) | C2A—C1A—B1—C1B | 156.2 (19) |
| C1—C2—C3—C4 | −0.1 (4) | C2A—C1A—B1—C1B$^{v}$ | −104.0 (3) |
| C1—C2—C3—C7 | 178.5 (3) | C2A—C1A—B1—C1B$^{vi}$ | 128.9 (4) |
| C1—C6—C5—C4 | 1.3 (5) | C2A—C3A—C4A—C5A | 3.2 (4) |
| C1—C6—C5—C8 | 178.5 (3) | C3A—C2A—C1A—C6A | −1.5 (3) |
| C1$^{i}$—B1—C1—C2 | 10.2 (2) | C3A—C2A—C1A—B1 | −176.95 (18) |
| C1$^{vi}$—B1—C1—C2 | 130.34 (18) | C3A—C4A—C5A—C6A | 0.6 (3) |
| C1$^{v}$—B1—C1—C2 | −109.51 (17) | C3A—C4A—C5A—C8A | −179.4 (4) |
| C1$^{i}$—B1—C1—C6 | −172.5 (2) | C5A—C4A—C3A—C7A | −174.8 (4) |
| C1$^{v}$—B1—C1—C6 | 67.8 (2) | C5A—C6A—C1A—B1 | −178.86 (17) |
| C1$^{vi}$—B1—C1—C6 | −52.4 (2) | C6A—C1A—B1—C1B$^{v}$ | 80.8 (3) |
| C1$^{v}$—B1—C1A—C2A | −108.2 (2) | C6A—C1A—B1—C1B$^{vi}$ | −46.2 (4) |
| C1$^{i}$—B1—C1A—C2A | 11.5 (2) | C6A—C1A—B1—C1B | −19.0 (19) |
| C1$^{vi}$—B1—C1A—C2A | 131.7 (2) | C6A—C1A—B1—C1B$^{i}$ | −170.5 (5) |

| | | | |
|---|---|---|---|
| C1$^{i}$—B1—C1A—C6A | −163.6 (2) | C1B—C2B—C3B—C4B | 5.6 (4) |
| C1$^{v}$—B1—C1A—C6A | 76.70 (18) | C1B—C2B—C3B—C7B | 178.0 (4) |
| C1$^{vi}$—B1—C1A—C6A | −43.45 (19) | C1B—C6B—C5B—C4B | −5.6 (4) |
| C1—B1—C1B—C2B | −23 (2) | C1B—C6B—C5B—C8B | −177.5 (4) |
| C1$^{vi}$—B1—C1B—C2B | 133.5 (2) | C1B$^{vi}$—B1—C1B—C2B | 130.5 (4) |
| C1$^{v}$—B1—C1B—C2B | −109.5 (3) | C1B$^{i}$—B1—C1B—C2B | 7.1 (5) |
| C1$^{i}$—B1—C1B—C2B | 14.2 (3) | C1B$^{v}$—B1—C1B—C2B | −106.0 (3) |
| C1$^{vi}$—B1—C1B—C6B | −44.7 (3) | C1B$^{i}$—B1—C1B—C6B | −171.1 (4) |
| C1$^{v}$—B1—C1B—C6B | 72.4 (3) | C1B$^{v}$—B1—C1B—C6B | 75.8 (4) |
| C1$^{i}$—B1—C1B—C6B | −164.0 (3) | C1B$^{vi}$—B1—C1B—C6B | −47.7 (4) |
| C1—B1—C1B—C6B | 159 (3) | C2B—C1B—C6B—C5B | 4.5 (4) |
| C2—C1—C6—C5 | −0.5 (3) | C2B—C3B—C4B—C5B | −5.9 (4) |
| C2—C1—B1—C1A$^{v}$ | −109.51 (19) | C3B—C2B—C1B—C6B | −4.7 (4) |
| C2—C1—B1—C1A$^{i}$ | 10.2 (3) | C3B—C2B—C1B—B1 | 176.99 (18) |
| C2—C1—B1—C1A$^{vi}$ | 130.3 (2) | C3B—C4B—C5B—C6B | 6.2 (4) |
| C2—C1—B1—C1B$^{i}$ | 3.3 (5) | C3B—C4B—C5B—C8B | 178.0 (4) |
| C2—C1—B1—C1B$^{vi}$ | 127.6 (4) | C5B—C4B—C3B—C7B | −178.5 (4) |
| C2—C1—B1—C1B$^{v}$ | −105.4 (3) | C5B—C6B—C1B—B1 | −177.26 (19) |

Symmetry codes: (i) −*y*+1, *x*−1/2, −*z*+2; (ii) −*y*+3/2, *x*, *z*; (iii) −*x*+1, −*y*+1, −*z*+1; (iv) *y*+1/2, −*x*+1, −*z*+1; (v) *y*+1/2, −*x*+1, −*z*+2; (vi) −*x*+3/2, −*y*+1/2, *z*.